

# RSC Advances

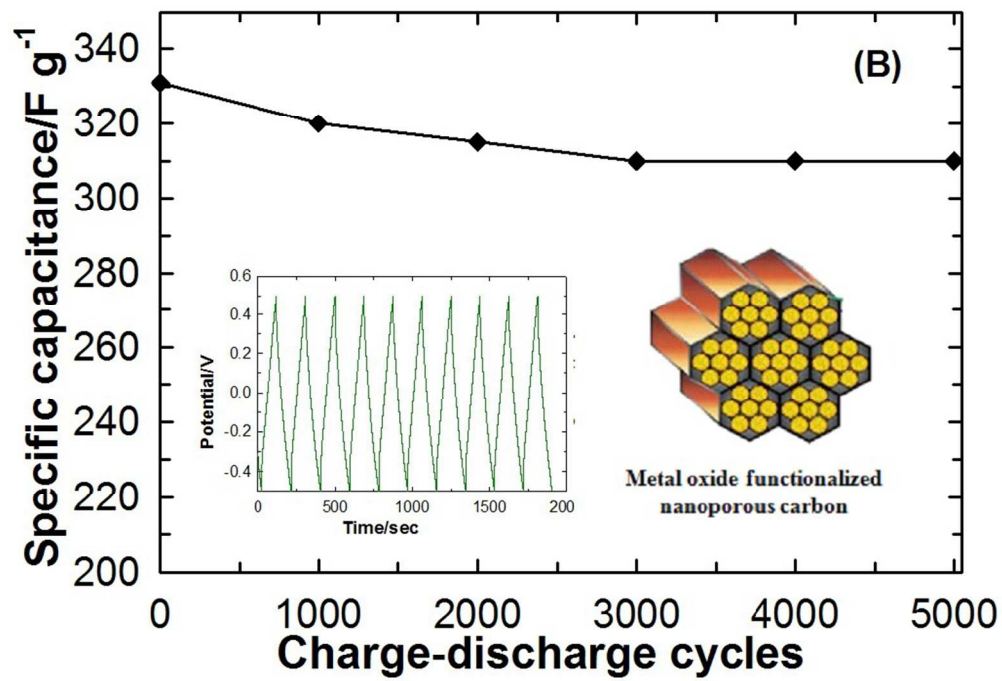


This is an *Accepted Manuscript*, which has been through the Royal Society of Chemistry peer review process and has been accepted for publication.

*Accepted Manuscripts* are published online shortly after acceptance, before technical editing, formatting and proof reading. Using this free service, authors can make their results available to the community, in citable form, before we publish the edited article. This *Accepted Manuscript* will be replaced by the edited, formatted and paginated article as soon as this is available.

You can find more information about *Accepted Manuscripts* in the [Information for Authors](#).

Please note that technical editing may introduce minor changes to the text and/or graphics, which may alter content. The journal's standard [Terms & Conditions](#) and the [Ethical guidelines](#) still apply. In no event shall the Royal Society of Chemistry be held responsible for any errors or omissions in this *Accepted Manuscript* or any consequences arising from the use of any information it contains.



173x131mm (150 x 150 DPI)

## ARTICLE

# Cobalt oxide functionalized nanoporous carbon electrodes and their excellent supercapacitive performance

Cite this: DOI: 10.1039/x0xx00000x

Received 00th January 2012,  
Accepted 00th January 2012

DOI: 10.1039/x0xx00000x

[www.rsc.org/](http://www.rsc.org/)

Dattatray S. Dhawale,<sup>a,b</sup> Gurudas P. Mane,<sup>b</sup> Stalin Joseph,<sup>a</sup> Siddulu N. Talapaneni,<sup>b</sup> Chokkalingam Anand,<sup>a,b</sup> Ajayan Mano,<sup>b</sup> Salem S. Aldeyab,<sup>c</sup> Kripal S. Lakhi,<sup>a</sup> and Ajayan Vinu<sup>\*a,b</sup>

Nanoporous carbon (CMK-3-150) functionalized with different amount of cobalt oxide (CoO) nanoparticles were synthesized by incipient wetness impregnation technique for supercapacitor application. The characterization results reveal that the specific surface area and pore volume of the CoO functionalized CMK-3-150 marginally decrease with increasing the amount of the CoO whereas the pore diameter and the structure of the CMK-3-150 were not affected even after the functionalization. The electrochemical measurements show that the specific capacitance of the electrodes enhanced after the functionalization with CoO. Among the electrodes studied, CMK-3-150 functionalized with 15 wt% CoO shows an excellent cycling stability and the specific capacitance of 331 F g<sup>-1</sup>, which is ca. two times higher than that of the pure nanoporous carbon. This enhanced performance is due to the combined contribution of electrical double layer capacitance and pseudocapacitance. A symmetric supercapacitor device based on CMK-3-150-15Co electrode gives the maximum energy density of 29.67 Wh kg<sup>-1</sup> at a power density of 0.07 kW kg<sup>-1</sup>.

## 1. Introduction

The research on the energy storage and conversion has been receiving much attention in the recent years owing to the decreasing availability of fossil fuels, the fast-growing demand for high-power applications such as electric and hybrid vehicles and the public awareness for the clean energy.<sup>1-3</sup> Among the energy storage devices, supercapacitors or electrochemical capacitors are considered as one of the promising options for next-generation power devices<sup>4</sup> due to their peculiar characteristics of high power density, fast charge/discharge rates, long cycle lifetime and safety compared against primary and secondary batteries.<sup>5,6</sup> However, the performance of the supercapacitors has to be improved in order to meet the ever-growing need for peak-power assistance in electric vehicles and other future system. This can only be achieved by developing novel electrode/support systems. Therefore, much attention has been paid to the design and development of new electrode materials for the supercapacitor applications.

Various carbon materials such as amorphous carbons to carbon nanotubes (CNTs) with a high specific surface area have been widely used as electrode materials for electrical double layer supercapacitors (EDLC) <sup>2-6</sup> whereas metal oxides such as RuO<sub>2</sub>, NiO, Co<sub>3</sub>O<sub>4</sub> and MnO<sub>2</sub> or conducting polymers have been generally considered for the faradaic pseudocapacitors.<sup>7-13</sup>

Although EDLCs based on pure carbon materials offer a very high degree of reversibility in repetitive charge/discharge cycling, they do not exhibit enough low specific capacitance and energy density because of the limitations of reversible ion absorption at the electrode/electrolyte interface which restrains their potential applications in various devices and make hurdles for commercialization.<sup>14</sup> On the contrary, pseudocapacitors based on metal oxides possess rather higher capacitance, in which fast and reversible faradic processes take place due to electro-active species<sup>15</sup> but a high cost of RuO<sub>2</sub> and a relatively poor electrochemical cycle life of NiO, CoO, Co<sub>3</sub>O<sub>4</sub> and MnO<sub>2</sub> greatly undermine their overall effectiveness for supercapacitor applications.<sup>7-13</sup> In addition, unsupported metal or metal oxide nanoparticles are generally not easy to handle and form aggregates under drastic conditions including oxidation and reduction. In addition, the agglomerated metal oxide particles significantly reduce the electronic conductivity which is crucial for the better electron transport system between the current collector and the electrode.<sup>16</sup> In order to develop supercapacitors, it is important to take the advantage from both the EDLCs and pseudocapacitors which has long cycle life time and high specific capacitance, respectively in a single system.

This can easily be achieved by functionalising the porous carbon electrodes with either metal oxides or conducting polymers. The development and progress of metal nitrides as suitable electrode materials for lithium-ion batteries and supercapacitors has been successfully demonstrated.<sup>17</sup> Recently, carbon-metal oxide composite materials as supercapacitor electrodes have well been documented in the literature.<sup>18</sup> Echegoyen et al. successfully enhanced the specific capacitance of carbon nano-onions by decorating with both pseudocapacitive redox materials, Ni(OH)<sub>2</sub> and NiO.<sup>19</sup>

In this study, it is planned to fabricate the hybrid electrodes by combining the high surface area porous carbon support system with a low cost metal oxide nanoparticles. Recently, Dhawale et al. demonstrated that CMK-3 as EDLCs electrodes which exhibit higher performance as compared to the commercially available multi-walled carbon nanotubes (MWCNTs) and activated carbon (AC). They also found that the combination of higher surface area and large pore diameter are critical to achieve a high specific capacitance (186 F g<sup>-1</sup>). Therefore, we have chosen CMK-3-150 as the supports for the supercapacitance studies. For the transition metal oxides, cobalt oxide is chosen as it is found to be very promising because of its abundance availability, good thermal and electrical conductivity, and environmentally benign nature. Although cobalt oxides showed amazing performance for supercapacitors, the reports on the fabrication of CMK-3-150 electrodes functionalized with cobalt oxide nanoparticles for energy storage are quite limited.<sup>20-22</sup>

Metal oxide nanoparticles can be introduced into the nanochannels of carbon either by direct or post-synthetic method. In the direct synthetic approach, mesoporous metallosilicate should be used as templates. Recently, Vinu et al. reported the direct incorporation of a high amount of metal ions in the mesoporous SBA-15 silica framework by simply adjusting the water-to-hydrochloric acid molar ratio of the synthesis medium without destroying the mesoporous structures.<sup>23</sup> They also converted the copper substituted mesoporous silica into mesoporous carbon with the copper oxide nanoparticles and studied their performance for supercapacitors.<sup>24</sup> Unfortunately, the preparation condition has a limitation that a high content of metal oxide nanoparticles in the mesoporous carbon support cannot be prepared as the HF treatment that is used for the removal of the silica, dissolves/removes the metal oxide nanoparticles from the porous channels. In addition, it is difficult to prepare mesoporous silica with a high metal content without affecting the mesoporous structure by the currently available direct synthesis route. These drawbacks limit the preparation of mesoporous carbon with a high amount of metal oxide nanoparticles in the mesochannels that make hurdles for obtaining high electrochemical performance.

In this study we report, functionalization of nanoporous carbon (CMK-3-150) electrodes with cobalt oxide (CoO) nanoparticles via post synthetic wet-impregnation pathway which allows the formation of the CoO nanoparticles on the surface of the nanoporous carbon support without affecting the structural order and the textural properties. The obtained materials have been characterized with various sophisticated techniques in order to analyze the structure and the textural parameters of the support before and after the functionalization with different amount of CoO nanoparticles and employed as

the electrodes for supercapacitor applications. It has been found that the amount of CoO nanoparticles play a critical role in enhancing the specific capacitance and the performance of the nanoporous carbon functionalized with CoO nanoparticles is superior to pristine nanoporous carbon electrodes.

## 2. Experimental Section

Tri-block copolymer P123 (EO<sub>20</sub>PO<sub>70</sub>EO<sub>20</sub>, EO = ethylene oxide, PO = propylene oxide, average molecular weight 5800) and tetraethyl orthosilicate (TEOS) were purchased from Aldrich. Analytical grade cobalt nitrate hexahydrate (Co(NO<sub>3</sub>)<sub>2</sub>·6H<sub>2</sub>O) was purchased from Wako Chemicals, Japan. All solvents were of analytical grade and used as received.

SBA-15 was synthesized using Tri-block copolymer P123. In a typical synthesis, 4 g of Pluronic P123 was added to 30 mL of water. After stirring for a few hours, a clear solution was obtained. Thereafter, 120 mL of 2 M HCl was added and the solution was stirred for another 2 h. Then, 9 g of TEOS was added and the resulting mixture was stirred for 24 h at 40 °C and subsequently heated for 48 h to 150 °C. The solid product was recovered by filtration, washed several times with water and dried overnight at 100 °C. Finally, the product was calcined at 540 °C to remove the surfactant. A mesoporous carbon was prepared by using SBA-15 prepared at 150 °C (SBA-15-150) as the template and sucrose as the carbon source.<sup>25, 26</sup> In a typical synthesis of mesoporous carbon, 1 g of SBA-15-150 was added to a solution obtained by dissolving 1.25 g of sucrose and 0.14 g of H<sub>2</sub>SO<sub>4</sub> in 5 g of water and keeping the mixture in an oven for 6 h at 100 °C. Subsequently, the oven temperature was raised to 160 °C for another 6 h. In order to obtain fully polymerized and carbonized sucrose inside the pores of the silica template, 0.8 g of sucrose, 0.09 g of H<sub>2</sub>SO<sub>4</sub> and 5 g of water were again added to the pre-treated sample and the mixture was again subjected to the thermal treatment described above. The template-polymer composites was then pyrolyzed in a nitrogen flow at 900 °C and kept under these conditions for 6 h to carbonize the polymer. The mesoporous carbon was recovered after dissolution of the silica framework in 5 wt% hydrofluoric acid by filtration, washed several times with ethanol and dried at 100 °C. The synthesized material was designated as CMK-3-150.

For the synthesis of CMK-3-150 with different amount of CoO nanoparticles (7, 10, 15, and 20 wt.%), a desired amount of Co(NO<sub>3</sub>)<sub>2</sub>·6H<sub>2</sub>O in 50 mL of ethanol was added to 0.1 g of CMK-3-150. The resulting mixture was sonicated for 1h followed by stirring the reaction mixture at room temperature for 24 h. The reaction mixture was then heated to 50 °C for 1 h while stirring and dried at 100 °C for 6 h. The resultant black colored powder was then subjected to calcination at 500 °C under a nitrogen flow for 5 h. A set of the samples was prepared by loading 7, 10, 15 and 20 wt% of cobalt oxide nanoparticles in CMK-3-150 and the samples are denoted as CMK-3-150-7Co, CMK-3-150-10Co, CMK-3-150-15Co and CMK-3-150-20Co, respectively. Powder X-ray diffraction (XRD) patterns of the samples loaded with different amount of CoO were recorded with a Rigaku diffractometer using CuK $\alpha$  ( $\lambda=0.154$  nm) radiation, in the 2 $\theta$  range of 0.6-10°, with a step of 0.01° and step time of 10 sec and for 2 $\theta$  range of 10-80°. N<sub>2</sub> adsorption and desorption isotherms were performed at -196 °C

with a Quantachrome Autosorb 1 sorption analyzer. The specific surface area was calculated using the Brunauer-Emmett-Teller (BET) method. The pore size was obtained from the adsorption and desorption branch of the nitrogen isotherms by the Barrett-Joyner-Halenda (BJH) method. The inductively coupled plasma atomic emission spectroscopy (ICP-OES) measurements were conducted using a Varian 720-ES instrument. Samples were first taken in aqua regia solution which is mixture of nitric acid and hydrochloric acid and digested in microwave and amount of CoO was detected. The surface morphology and composition of the materials were studied with a Hitachi S-4800 field-emission high-resolution scanning electron microscope (HRSEM, accelerating voltage 5.0 kV). Transmission electron microscopy (TEM) of the samples was carried out using a Titan G2 80-300 ST microscope from FEI Company (Hillsboro, OR) that was equipped with an EDS detector, a post-column energy filter, and charged-coupled devices (CCD) camera. Furthermore the analysis was performed by operating the microscope at 300 kV but setting it to different image magnifications and a few TEM-modes. First of all, TEM specimens of samples were prepared by placing a small amount on holey-carbon coated gold (Cu) grids. The EDS analysis was performed next to investigate the elemental composition of samples. High-angle annular dark-field scanning transmission electron microscopy (HAADF-STEM) analysis of samples was used to verify the formation of CoO nanoparticles. Finally elemental mapping of Co, O, and C was performed with a post-column energy-filter of model GIF Tridiem from Gatan Inc. It was in fact completed by acquiring M-45, O-K, and C-K edges of Co, O, and C elements, respectively. Furthermore the so-called 3-window method was utilized to generate these elemental maps.

A bare glassy carbon electrode (GCE) was mirror-polished with 0.05 M Al<sub>2</sub>O<sub>3</sub> slurry and rinsed with double-distilled water. The electrode materials were dispersed in an aqueous solution of dehydrated ethanol and sonicated for 20 min. Then 20  $\mu$ L of slurry was spread onto the GCE surface using a micropipette and the electrodes were dried at 70 °C for 1 h to evaporate the solvent. Electrochemical supercapacitor performance was carried out with a CHI 760D workstation in a standard three-electrode cell configuration. CoO loaded CMK-3, platinum wire and SCE were used as working, counter and

reference electrodes, respectively. The measurements were carried out in a 1 M Na<sub>2</sub>SO<sub>4</sub> aqueous electrolyte solution by cyclic voltammetry technique within a potential window -0.5 and 0.5 V (Vs. SCE) at a different scan rates ranging from 5 to 40 mV s<sup>-1</sup>. The charge-discharge study was carried at 3 A g<sup>-1</sup> current density. Electrochemical impedance study was carried out at an open circuit potential and the data were collected in the frequency range of 10<sup>5</sup>-10<sup>-2</sup> Hz with AC amplitude of 5 mV. The electrochemical performance of the symmetric supercapacitor cell with both the positive and negative electrode of CMK-3-150-15Co was investigated by CV at the scan rate of 5 mV s<sup>-1</sup> and charge-discharge curves at different current densities based on the mass loading of the electrodes was varied from 0.3 A g<sup>-1</sup> to 6.6 A g<sup>-1</sup> to evaluate specific and power density of the device.

### 3. Results and Discussion

The structural order of the nanoporous carbon before and after the loading of CoO nanoparticles was obtained by low-angle powder X-ray diffraction (XRD) measurements whereas the crystallinity and the agglomeration of the formed CoO nanoparticles along the pore channels were measured by wide-angle powder XRD. **Fig. 1A** shows the low angle XRD patterns of the samples with different amount of CoO nanoparticles prepared by post-synthetic route. All the samples showed a main peak at lower angle, indicating that the functionalized samples possess ordered mesoporous structure and the structural stability is retained even after the incorporation of CoO nanoparticles inside nanoporous carbon support. **Fig. 1B** shows the wide angle powder XRD patterns of CMK-3-150 functionalized with 7, 10, 15 and 20 wt% of CoO nanoparticles. As can be seen in **Fig. 1B**, all the samples except CMK-3-150-20Co showed either no or broad peaks at higher angles, revealing that the CoO oxide particles are not agglomerated and finely dispersed inside the mesochannels. The low peak intensity of the CMK-3-150-7, 10 and 15Co materials confirming the formation of small crystal size of CoO and is due to the fact that the pore diameter of the support helps to control the size of the nanoparticles whereas the well-ordered mesostructure and the high surface supports the growth and fine dispersion of CoO nanoparticles inside the mesochannels. However, when the loading was increased from 15 to 20wt.%, sharp peaks related to CoO nanoparticles were appeared and the crystallite size of the particles calculated from Debye-Scherrer's formula is ca. 20 nm. These results indicate that most of the

**Table 1:** Textural parameters, values of specific and areal capacitance and CoO wt% by ICP analysis of CMK-3-150-7Co, CMK-3-150-10Co, CMK-3-150-15Co and CMK-3-150-20Co electrodes.

Electrode Materials	Surface area/ m <sup>2</sup> g <sup>-1</sup>	Pore volume/ cc g <sup>-1</sup>	Pore diameter/nm	Specific capacitance/ F g <sup>-1</sup>	Areal capacitance/F cm <sup>-2</sup>	CoO wt % by ICP
CMK-3-150-7Co	1137	1.33	6.6	190	0.26	6.509
CMK-3-150-10Co	818	1.16	6.6	297	0.53	9.142
CMK-3-150-15Co	760	1.12	6.6	331	0.59	14.452
CMK-3-150-20Co	685	1.01	6.4	200	0.35	18.383

particles are formed on the external surface of the nanoporous carbon when the amount of CoO is higher than 15 wt.%, which is mainly due to the agglomeration of nanoparticles at high temperature.

increasing the loading of CoO nanoparticles in the mesochannels. This is expected because the surface of the carbon walls is covered by highly dense CoO nanoparticles which not only affect the surface area but also the total weight of the samples. The specific surface area decreases from 1137 to 685  $\text{m}^2 \text{g}^{-1}$  with increasing the loading of CoO content from 7 to 20 wt.% in the nanoporous carbon support, respectively. In addition, the pore diameter and pore volume also decrease with increasing the content of CoO (Table 1). It should be noted that the reduction of pore volume and the specific surface area of CMK-3-150-20Co is much higher than that of other samples studied in this work. This could be due to the fact that the large CoO crystals that are formed on the external surface of the carbon supports block the primary mesochannels, resulting in a huge reduction of specific surface area. This is also reflected in the results obtained from powder XRD measurements.

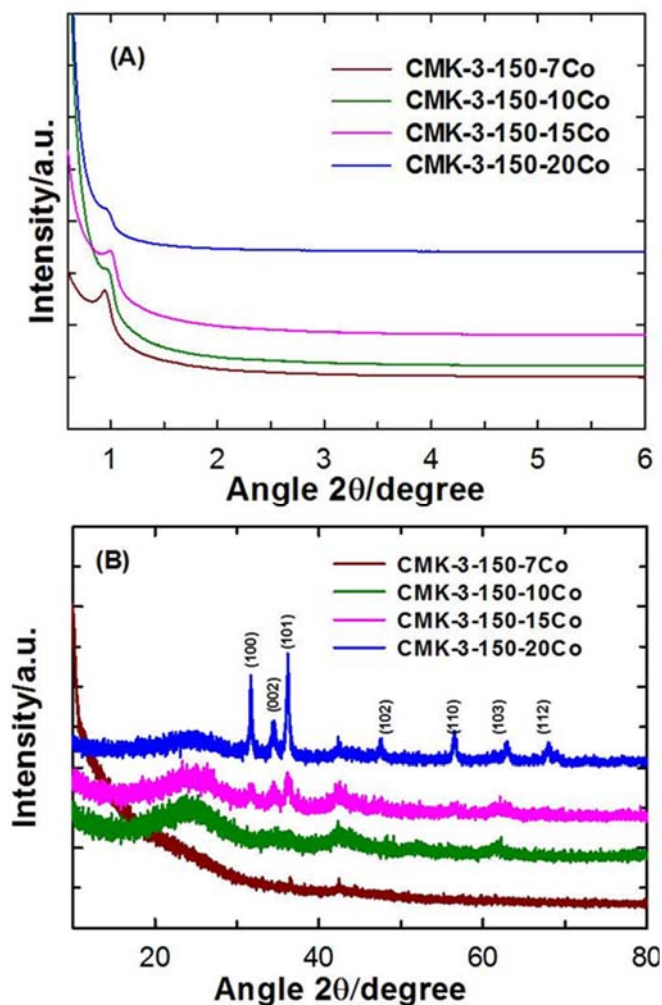


**Fig. 1** (A) Low (A) and (B) wide angle XRD patterns of CMK-3-150-7Co, CMK-3-150-10Co, CMK-3-150-15Co and CMK-3-150-20Co.

The specific surface area, pore volume and pore diameter of the CoO nanoparticles functionalized nanoporous carbons were obtained by nitrogen adsorption-desorption measurements. **Fig. 2A** and **2B** display the nitrogen adsorption isotherms and the pore size distribution of mesoporous carbon loaded with different amount of CoO nanoparticles, respectively. The entire samples exhibit type IV isotherm with a sharp capillary condensation step and a broad  $H_1$ -type hysteresis loop.<sup>23</sup> The shape of the isotherm and the capillary condensation step is almost similar to that of the pure nanoporous carbons, revealing that the mesoporosity of the samples are not affected even after the encapsulation of the CoO nanoparticles. The textural parameters such as BET specific surface area, pore diameter based on BJH analysis and specific pore volume of the samples are summarized in Table 1. It should be noted that amount of the nitrogen adsorbed at the monolayer region of the isotherm which is directly related to the specific surface area of the samples which is decreases with

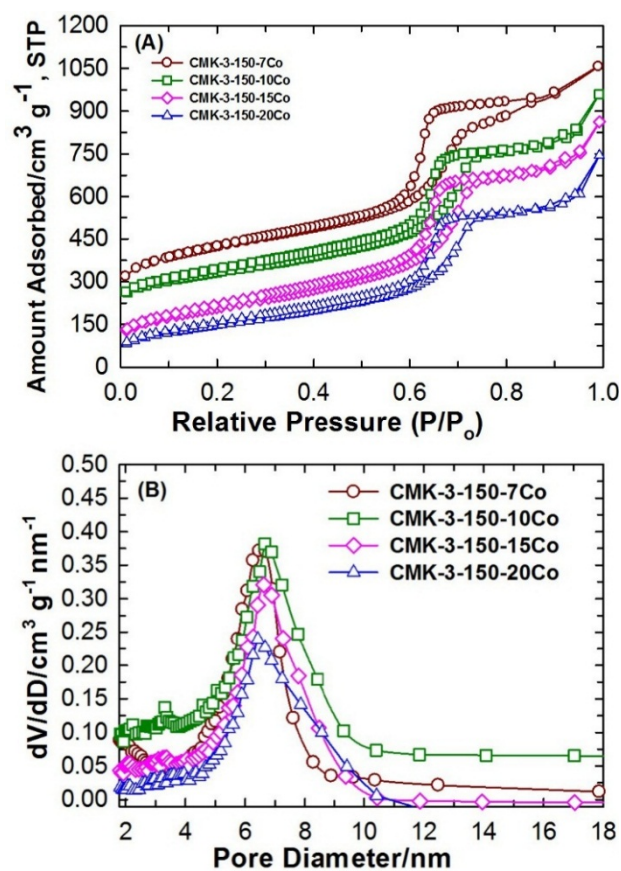


**Fig. 2.** (A) Nitrogen isotherm and (B) pore size distribution of CMK-3-150-7Co, CMK-3-150-10Co, CMK-3-150-15Co and CMK-3-150-20Co (Isotherms are shifted upwards for clarity).

In order to understand the effect of different CoO wt% on the morphology of nanoporous carbon support and verify the formation of CoO nanoparticles on the surface of the support, the samples were subjected to high resolution scanning electron microscopic (HRSEM) measurements. HRSEM images at two different magnifications of (A, B) CMK-3-150-7Co, (C, D) CMK-3-150-10Co, (E, F) CMK-3-150-15Co and (G, H) CMK-3-150-20Co, respectively are presented in **Fig. 3**. As can be seen from the **Fig. 3**, the entire samples display rod like morphologies which are typically observed for the nanoporous

carbon prepared from SBA-15 template. The crystalline nanoparticles were detected by the HRSEM measurements and these nanoparticles could be seen as white colored dots in the HRSEM images, that increase with increasing the loading of CoO nanoparticles in the support. The white spots on all the images correspond to the CoO nanoparticles which are finely dispersed on the surface of the support and increases with increasing CoO content. In addition, no difference in the morphology of the materials upon changing the CoO content in the synthesis mixture also confirms the retention of the structural and morphological order after the incorporation of the large amount of CoO nanoparticles. These results reveal that the stability of the support and the oxygen from the Co source did not make any damage to the morphology. The HRSEM images in Fig. 3 also indicate that the nanoparticles are randomly oriented inside the mesochannels of the support. Moreover, the nanoparticles are highly dispersed and located not only on the external surface but also inside the walls and pores of the samples.

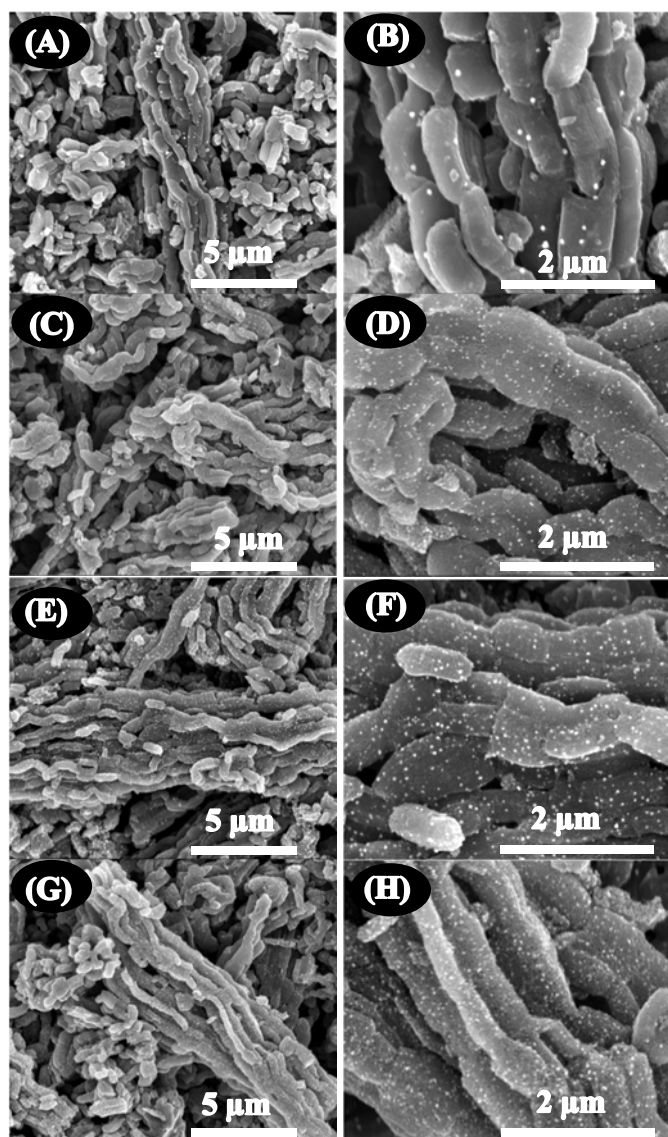


**Fig. 3.** HRSEM images at two different magnifications of (A, B) CMK-3-150-7Co, (C, D) CMK-3-150-10Co, (E, F) CMK-3-150-15Co and (G, H) CMK-3-150-20Co.

**Fig. 4 (A, C, E, G)** and **Fig. 4 (B, D, F, H)** show the HRTEM and scanning transmission electron microscopy high-angle annular dark field (HAADF) images of the CoO functionalized nanoporous carbon having different CoO content, respectively. The HRTEM images display that the support materials exhibit well-ordered

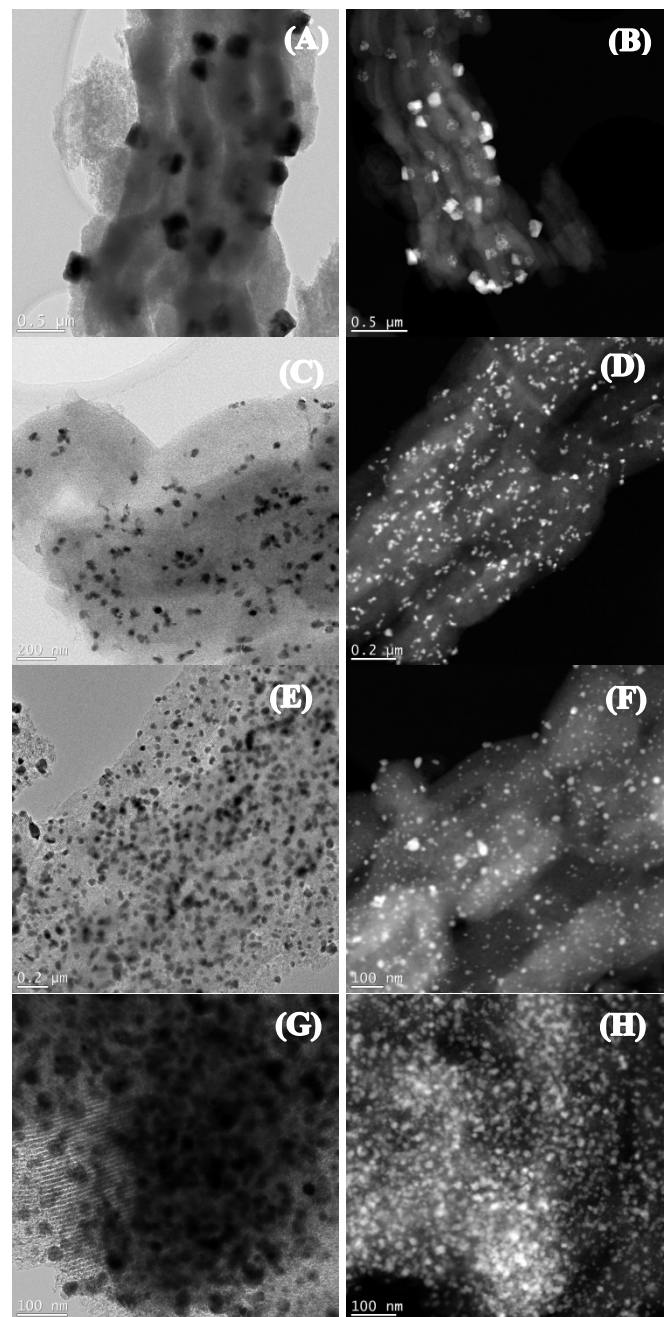


**Fig. 4.** HRTEM (A, C, E, G) and scanning transmission electron microscopy HAADF (B, D, F, H) images of CMK-3-150-7Co, CMK-3-150-10Co, CMK-3-150-15Co and CMK-3-150-20Co, respectively.

mesoporous structure even after the loading of CoO nanoparticles. All the samples consist of equidistant and parallel nanopore arrays that are similar to the structure of pure

mesoporous carbon, revealing that the structure of the mesoporous carbon is stable despite the encapsulation of a high amount of CoO in the nanochannels. The nanoparticles could be seen as black spots in the HRTEM images and are highly dispersed throughout the samples. From these results, it is clear that the large nanoparticles are formed on the external surface whereas the small nanoparticles are grown inside the mesochannels. Thus, it can be concluded that an optimized control of the CoO percentage is highly necessary to preserve the mesoporous structure of carbons with a very high ordering and good textural parameters. It should be noted that the CoO nanoparticles in CMK-3-150-20Co which has the highest content of CoO get agglomerated and block the pores and thereby may resist the free transportation of the ions. Using scanning transmission electron microscopy with aberration corrector in probe, HAADF images of CMK-3-150-7Co, CMK-3-150-10Co, CMK-3-150-15Co and CMK-3-150-20Co, were obtained (Fig. 4 B, D, F, H). From the HAADF images also clear that the white spots of CoO nanoparticles increases as the CoO amount increases from 7 to 20 wt % in the nanoporous support. Among the samples studied in the present work, CMK-3-150-20 shows the higher amount of CoO nanoparticles and get agglomerated which blocks the pore channels of the support. The HRTEM and HAADF results are highly reflected in HRSEM images of the electrodes. Therefore, a fine control of the CoO in the nanochannels is highly critical to achieve the best performance in the energy storage devices. We assume that the mesopores of the support are quite large in size which is extremely helpful for transportation of the ions from the electrolytes to enhance the electrochemical performance.

The presence of the CoO nanoparticles and their distribution on the surface of the nanoporous carbon support have also been analyzed by HRTEM-energy-dispersive X-ray spectroscopy (EDS). Fig. 5 (A) shows the EDS spectra of CMK-3-150-7Co, 10Co, 15Co and 20Co whereas the Fig. 5. (B) shows elemental mapping of CMK-3-150-15Co for C, O and Co elements. All the materials exhibit four sharp peaks which clearly indicate the presence of C, O and Co. The peak at the lowest keV corresponds to C from the nanoporous support whereas the peak at 0.5 KeV corresponds to O from the CoO. The two peaks centered at 0.75 and 6.9 keV are attributed to the main Co. It is interesting to note that the intensity of the peak for Co increases with increasing the loading of the CoO nanoparticles, which reveals the perfect incorporation of metal oxide nanoparticles inside the nanochannels of nanoporous carbon support. The elemental mapping reveals that the particles are not agglomerated on the surface of the nanoporous carbon support which is mainly due to the high surface area and large pore diameter of the support. The inductively coupled plasma atomic emission spectroscopy (ICP-AES) measurement revealed that the amount of CoO increases with increasing the amount of Co in the nanoporous carbon support from 7 to 20 wt%, which is also consistent with the data obtained from the EDS measurements. The absence of the signals of F and S indicates that the samples are free from these elements and the samples are washed perfectly after the silica removal with hydrofluoric acid. From the elemental mapping, it is clear that the Co and O are uniformly distributed over the surface of the samples. These results confirm the presence of the CoO nanoparticles on the surface of the mesoporous carbon support, which are finely distributed on the porous channels of the support.

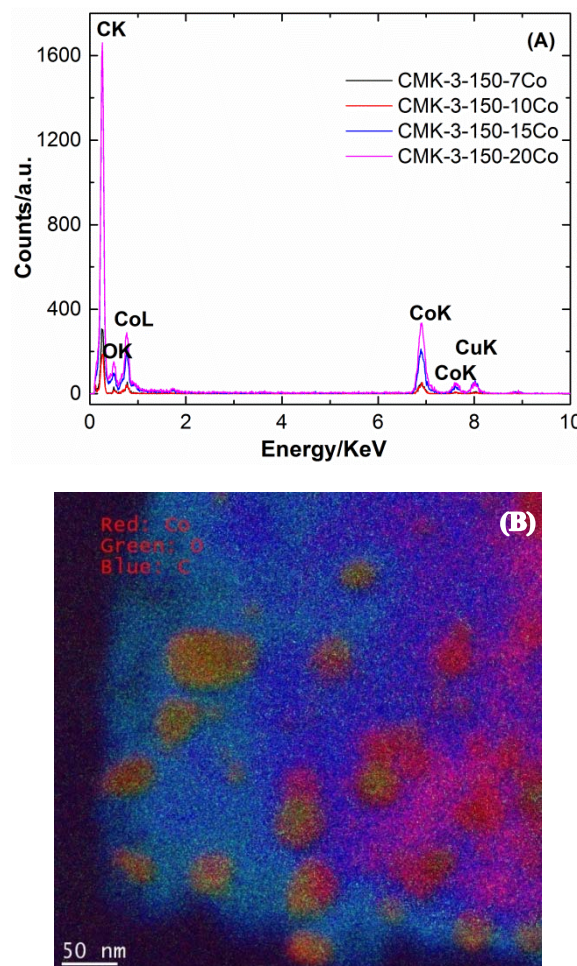


**Fig. 5.** Combined EDS spectra of (A) CMK-3-150-7Co, 10 Co, 15 Co and 20Co, (B) Elemental mapping of CMK-3-150-15Co.

The electrochemical measurements were carried out in a beaker type electrochemical half-cell setup equipped with an SCE (saturated KCl) reference electrode and a platinum wire counter electrode. The working electrodes were immersed in the electrolyte for 1 h to ensure that the electrode materials were thoroughly wet. Cyclic voltammetry (CV), chronopotentiometry for charge-discharge and electrochemical impedance study (EIS) which are effective tools to present the capacitive behaviour of electrode material were carried out using CHI 760D electrochemical workstation. The electrolytes used in the supercapacitors must have a maximum possible decomposition voltage and should be electrochemically stable. In addition, the resistance of the supercapacitor cell is dependent on the resistivity of the electrolyte and size of the ions from the electrolyte that diffuse into and out of the pores of the electrode particles. We have preferred the aqueous electrolytes as they are cheaper, easier to purify and have a lower resistance.<sup>27</sup> In the present case, 1 M Na<sub>2</sub>SO<sub>4</sub> aqueous electrolyte was used to study the electrochemical performance of the CMK-3-150-7Co, CMK-3-150-10Co, CMK-3-150-15Co and CMK-3-150-20Co and corresponding CV curves recorded at the scan rate of 5 mV s<sup>-1</sup> are displayed in Fig. 6. In the CV curves, cathodic peak is observed for all the electrodes, indicating that the capacitance is generated from the combination of both the EDLCs based on CMK-150 and pseudocapacitance based on CoO through a redox mechanism.

In addition, the CV curves are relatively flat and rectangular, which is typical for electrochemical double-layer capacitors. The combined effect of the EDLC and pseudocapacitance offered a maximum current that is clearly reflected on the total specific capacitance of the materials. It is also seen that the presence of the ultra-fine CoO oxide nanoparticles helps to enhance the conductivity of the electrode and thereby enhancing the transport of the electrons and further the contact between the current collectors and the electrode materials.

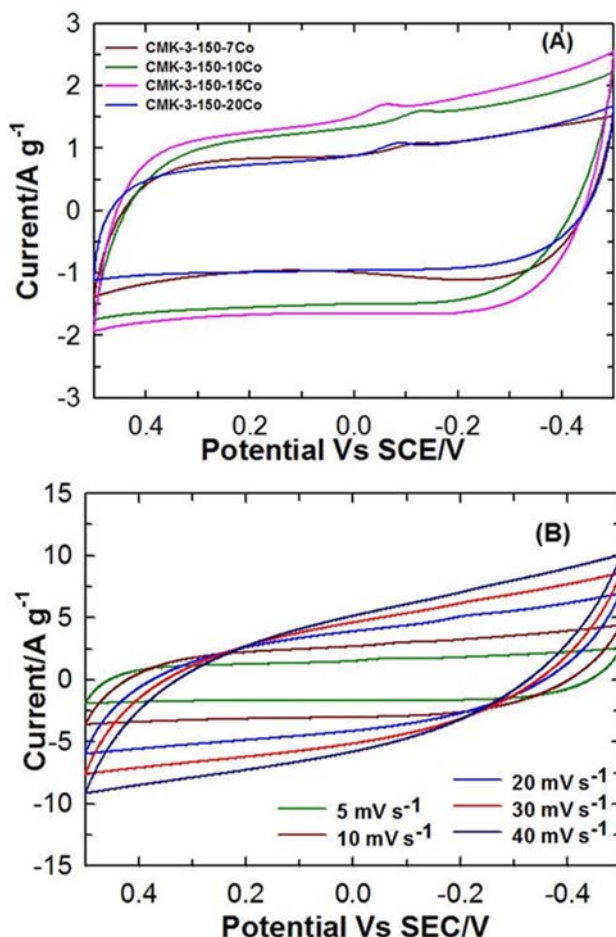


**Fig. 6.** (A) CV curves of CMK-3-150-7Co, CMK-3-150-10Co, CMK-3-150-15Co and CMK-3-150-20Co at  $5 \text{ mV s}^{-1}$  and (B) CV curves of CMK-3-150-15Co at different scan rates in  $1 \text{ M Na}_2\text{SO}_4$  electrolyte solution.

As can be seen from the CV curves, current response increases as the CoO content increases from 7 to 15 wt% in nanoporous carbon support and then starts to decrease when the CoO content reaches 20 wt%. From the CV curve, it is clear that the maximum current response is observed for CMK-3-150-15Co electrode which results in superior electrochemical performance. The significant improvement in electrochemical performance might result from the rod-like morphology of the carbon support, better textural parameters and the ultrafine and well-dispersed CoO nanoparticles. The well-ordered structure and the high surface area of the support help to access all the electrochemical active surface areas by the electrolyte ions and the redox sites for the surface reaction for the enhancement of

electrochemical performance. In addition, more pseudocapacitance contribution comes from the CoO nanoparticles that store charge through the transfer of charge between the electrode and the electrolyte with the help of electroadsorption, redox reaction and intercalation process. The high surface area of the support also gives the access to the electrolyte ions that further enhances the surface reaction and thereby enhancing the pseudocapacitance. This enhanced electrochemical performance of CMK-3-150-15Co electrode is likely a result of both the accessibility of the CoO in the nanoporous carbon framework and the electrical conductivity imparted by the continuous carbon framework. The decrease in electrochemical performance for CMK-3-150-20Co electrode could be due to the presence of the large aggregated CoO nanocrystals, as confirmed by XRD, and the lower surface area of the nanoporous carbon support (see Table 1). In addition, the blockage of the pore channels by these large particles could hinder the diffusion of the electrolyte ions inside the mesochannels and access the interior part of the pores, which is clearly reflected in the registered capacitance of the materials.

The effect of scan rate on the CV response of the CMK-3-150-15Co electrode was investigated over the range  $5\text{--}40 \text{ mV s}^{-1}$  as shown in Fig. 6B. The voltammetric currents are directly proportional to the scan rate, indicating an ideally capacitive behaviour. In addition, the shape of the CV curves is slightly distorted upon increasing the scan rate. At  $5 \text{ mV s}^{-1}$  scan rate, a near rectangular shape with a cathodic peak corresponds to CoO is observed. As the scan rate increases, the CV curves deviate from their original shape and the observed cathodic peak also disappears which indicates that the electrode starts to exhibit a small resistive behaviour at a high scan rate. In addition, the shape is slightly distorted at a high scan rate which is mainly due to a significant contribution of the equivalent series resistance (ESR) which is the slope of the  $V/I$  and associated with the capacitor.<sup>28</sup>

It is well accepted that charge-discharge examination is an established method for estimating the supercapacitive performance. Fig. 7A shows the charge-discharge profiles of the different wt% of CoO functionalized nanoporous carbon electrodes such as CMK-3-150-7Co, CMK-3-150-10Co, CMK-3-150-15Co and CMK-3-150-20Co at a current density of  $3 \text{ A g}^{-1}$ . The charge curves are symmetric to their corresponding discharge counterparts in the potential window, which indicates a good electrochemical stability and the feasibility of the CoO functionalized nanoporous carbon electrodes system for the development of supercapacitors. However, an initial drop in potential is observed, which is caused by internal resistance. When the charge-discharge profiles of the mesoporous carbons with different amounts of CoO nanoparticles are compared, the CMK-3-150-15Co electrode exhibits sharper slopes with lesser IR drop as compared with those of CMK-3-150-7Co, CMK-3-150-10Co and CMK-3-150-20Co electrodes. These results are consistent with the results obtained from CV curves.

The charge-discharge time of CMK-3-150-15Co electrode is significantly longer than that of other samples, resulting in higher capacitance. From this study, it can be concluded that the CMK-3-150-15Co electrode is a high performance supercapacitor than that of CMK-3-150-7Co, CMK-3-150-10Co and CMK-3-150-20Co electrodes. The specific capacitance  $C_s$  ( $\text{F g}^{-1}$ ) and areal capacitance  $C_i$  ( $\text{F cm}^{-2}$ ) of all the electrodes were calculated from the charge-discharge curves using the following relation<sup>24</sup> and values are given in Table 1,

$$C_s = I \times t_D / E \times W \quad (1)$$

$$C_i = I \times t_D / E \times A \quad (2)$$

Where,  $I$  is charge/discharge current at a discharge time  $t_b$ (s),  $E$  is the voltage range in (V),  $A$  is the geometrical area of electrode active material dipped in the electrolyte in ( $\text{cm}^2$ ) and  $W$  is the weight of active materials in (g). The specific capacitance of the CMK-3-150-15Co electrode ( $331 \text{ F g}^{-1}$ ) is much higher than that of the CMK-3-150-7Co ( $190 \text{ F g}^{-1}$ ), CMK-3-150-10Co ( $297 \text{ F g}^{-1}$ ) and CMK-3-150-20Co ( $200 \text{ F g}^{-1}$ ) electrodes at a current density of  $3.3 \text{ A g}^{-1}$ . Similarly, the areal capacitance of the electrodes also follows the same trend. The areal capacitance of CMK-3-150-15Co is  $0.59 \text{ F cm}^{-2}$  which is higher than that of the CMK-3-150-7Co ( $0.26 \text{ F cm}^{-2}$ ), CMK-3-150-10Co ( $0.53 \text{ F cm}^{-2}$ ) and CMK-3-150-20Co ( $0.35 \text{ F cm}^{-2}$ ) electrodes (Fig. 7B). This may be due to the fact that the addition of large amount of CoO nanoparticles favours agglomeration that would block the pore channels and affect

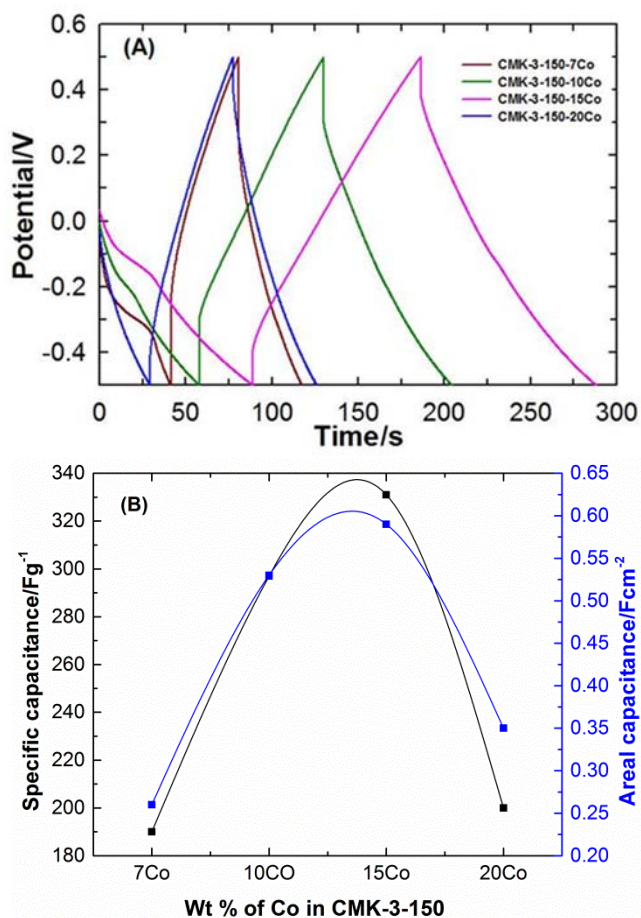


**Fig. 7.** (A) Charge-discharge curves 1 M  $\text{Na}_2\text{SO}_4$  electrolyte solution and (B) Variation of specific capacitance and areal capacitance at a  $3.3 \text{ A g}^{-1}$  current density of CMK-3-150-7Co, CMK-3-150-10Co, CMK-3-150-15Co and CMK-3-150-20Co electrodes.

the adsorption and redox process as well as the conductivity of the whole electrode.<sup>29</sup> It should be noted that the specific capacitance value reported in the present study is much higher than that of the activated carbon ( $55 \text{ F g}^{-1}$ ), multiwalled carbon nanotubes ( $22 \text{ F g}^{-1}$ ), pristine nanoporous carbons ( $186 \text{ F g}^{-1}$ ) and nitrogen doped nanoporous carbon ( $254 \text{ F g}^{-1}$ )<sup>30,31</sup> as shown in Fig. S1. This could be due to the combination of

EDLC and pseudocapacitance that is generated through the CoO nanoparticles in the wall structure of the mesoporous carbon support, and the uniform rod like morphology with long structural order even after the encapsulation of huge amount of CoO nanoparticles, very high specific surface area, large pore diameter and huge pore volume. These factors offer a low-resistant pathway for the ions through the porous structure and a shorter diffusion route due to interconnected mesochannels, and thereby enhance the specific capacitance.

Electrochemical impedance spectroscopy (EIS) is widely used to gain a deeper insight into electrochemical systems. AC impedance test of all the electrodes is carried out at an open circuit potential in the frequency range  $10^5$ - $10^{-2}$  Hz using a sinusoidal signal of 5 mV, where  $Z'$  and  $Z''$  are the real and imaginary parts of the impedance, respectively. The EIS graph presented in Fig. 8A gives the AC impedance spectra of the four electrodes namely CMK-3-150-7Co, CMK-3-150-10Co, CMK-3-150-15Co and CMK-3-150-20Co. Nyquist plots consist of a depressed semicircle in high-frequency region presenting the charge transfer resistance<sup>33</sup> and linear slopes in low frequency region characterized by purely capacitive behaviour.<sup>34</sup> At high frequencies, capacitance is negligible and resistance is dominant. A bigger semicircle means larger charge-transfer resistance and higher slope signifies lower diffusion rate. It is noted that all four electrode materials exhibit a smaller semicircle component at high frequency followed by lower slope component at the lower frequency, indicating that all electrodes have smaller charge transfer resistance and faster ion diffusion rate, which are consistent with the CV and charge-discharge results. The bulk electrolyte resistant can be found from the real impedance x-intercept of the Nyquist plot at high frequencies<sup>35,36</sup> is almost same for all the electrodes and is found to be  $2.86 \Omega$ . The value of the charge transfer resistance for CMK-3-150-15Co electrode ( $6 \Omega$ ) is smaller than the values of CMK-3-150-7Co ( $24 \Omega$ ), CMK-3-150-10Co ( $9 \Omega$ ) and CMK-3-150-20Co ( $16 \Omega$ ) electrodes. Also the radius of depressed semicircle of the CMK-3-150-15Co decreased at high frequency means the charge-transfer resistance is markedly decreased, indicating CMK-3-150-15Co electrode exhibits faster ion diffusion as compared with the other three electrodes. These results clearly reveal that the optimization of the CoO content in the mesoporous channels is very important in order to achieve the best electrochemical performance.

Cycling performance, which includes cycling capability or cycling life and capacitance retention, is another important characteristic of an electrochemical capacitor especially if pseudo-capacitance exists. Fig. 8B represents the plot of specific capacitance as a function of the charge-discharge cycle number of the CMK-3-150-15Co electrode examined by chronopotentiometry at a current density of  $3 \text{ A g}^{-1}$ . A total 5000 cycles in the potential range of  $-0.5$  to  $0.5 \text{ V}$  is measured and the charge-discharge curves upto 10 cycles are presented in the inset of Fig. 8B. For comparison, we performed stability by CV studies and the corresponding CV curves for 1<sup>st</sup> and after 5000<sup>th</sup> cycles at the scan rate of  $5 \text{ mV s}^{-1}$  also presented in the inset of Fig. 8B. It can be observed that the specific capacitance decreases gradually in the first 1000 cycles and remains constant thereafter. Additionally, capacity retention is very high and the loss in specific capacitance based on the maximum value after 5000 cycles is only 9%. The high cycling stability of CMK-3-150-15Co electrode is possible only because of the robust support with a highly stable carbon walls decorated with CoO nanoparticles. The porous structure also helps to retain the

nanoparticles in the mesochannels and its crystalline structure. These results also reveal that the redox surface reaction did not make any adverse effect on the wall structure of the mesoporous carbon support. Overall, the CoO loaded mesoporous carbons are excellent electrode system that offer much better electrochemical performance than the pure mesoporous carbon with tunable pore diameters. The combination of pseudocapacitance and the EDLC is crucial to increase the specific capacitance of the hybrid porous carbon electrodes.

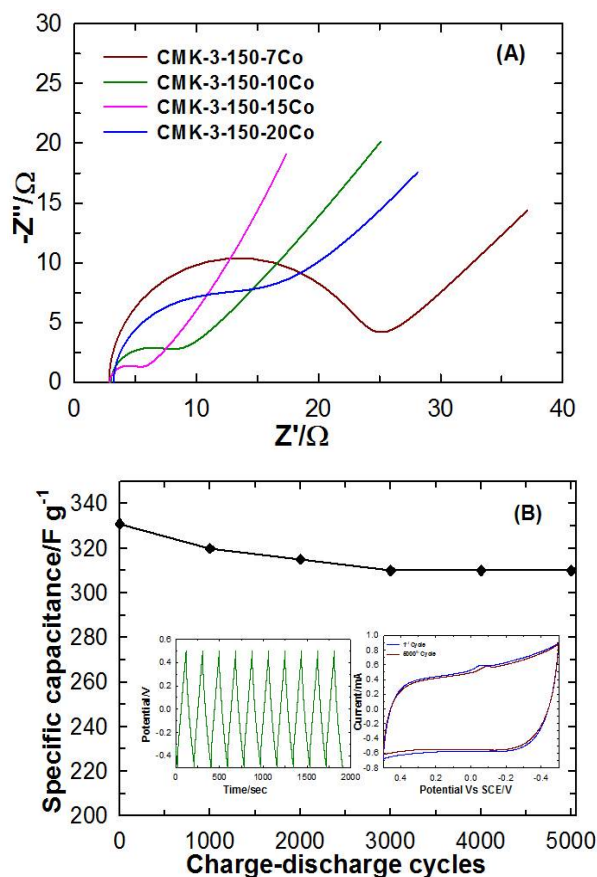


**Fig. 8** (A) Impedance plot of CMK-3-150-7Co, CMK-3-150-10Co, CMK-3-150-15Co and CMK-3-150-20Co and (B) Stability studies of CMK-3-150-15Co electrode 1 M Na<sub>2</sub>SO<sub>4</sub> electrolyte solution.

**Fig. 9A** shows the CV curves of a symmetric supercapacitor with both the positive and negative electrodes of CMK-3-150-15Co materials. The symmetric device was cycled with the cell voltage varying from 1.5 to 1.7 V at a sweep rate of 5 mV s<sup>-1</sup>. The chronopotentiometric charge-discharge curves of CMK-3-150-15Co symmetric supercapacitor with a cell voltage of 1.7 V at different current densities varying from 0.3 to 6.6 A g<sup>-1</sup> are presented in Fig. 9B. The charge-discharge profiles are in linear shape, demonstrating ideal capacitive behavior of symmetric cell. The energy density (storage capacity) and power density (rate of charge-discharge) are the two important fundamental parameters for power applications of electrochemical supercapacitors.

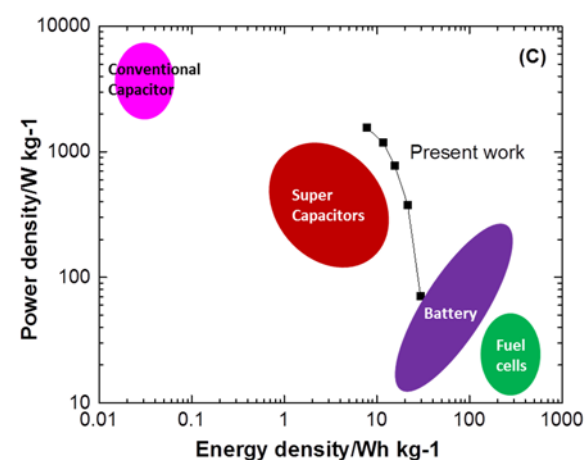
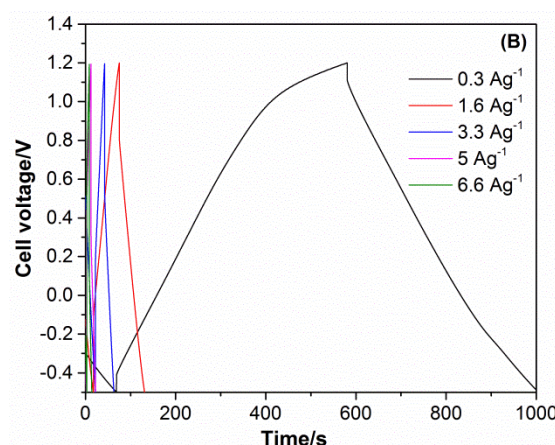
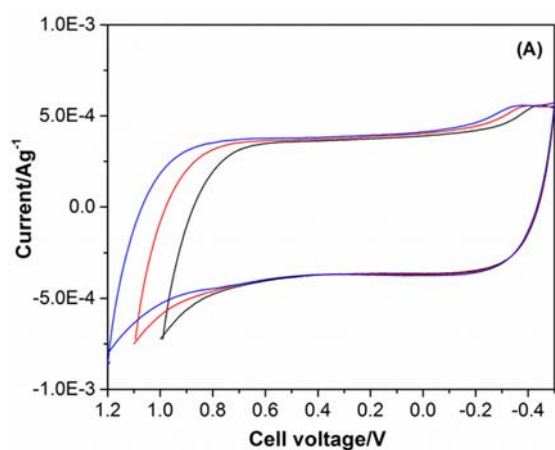


**Fig. 9** (A) CV of a symmetric supercapacitor cell based on CMK-3-150-15Co. The device was cycled with the upper cell voltage varying from 1.5 to 1.7 V at the scan rate of 5 mV s<sup>-1</sup> 1 M Na<sub>2</sub>SO<sub>4</sub> electrolyte solution (B) The chronopotentiometric charge-discharge curves of CMK-3-150-15Co symmetric supercapacitor with a cell voltage of 1.7 V at varying current densities from 0.3 to 6.6 A g<sup>-1</sup> (C) Ragone plot of CMK-3-150-15Co symmetric supercapacitor cell.

The energy and power densities were calculated using the below well-known equations (3) and (4), respectively<sup>32</sup>,

$$d_E (\text{Wh kg}^{-1}) = 0.5 C_s E^2 \times 1000/3600 \text{ ----- (3)}$$

$$d_P (\text{kW kg}^{-1}) = d_E/t_D \text{ ----- (4)}$$

The energy density and power density values of CMK-3-150-15Co electrode are calculated from the symmetric electrode configuration of the chronopotentiometric charge-discharge profiles at different current densities and their corresponding Ragone plot is plotted and compared with the standard Ragone plot<sup>37</sup> as shown in Fig. 9C. The obtained values for energy and power densities are higher than those of conventional supercapacitors in Ragone plot. From the Ragone plot of CMK-3-150-15Co symmetric supercapacitor, it is seen that the specific energy decreased from 29.67 to 7.79 Wh kg<sup>-1</sup> when the current density was increased from 0.3 to 6.6 Ag<sup>-1</sup>. These obtained values are higher than those of conventional supercapacitors in Ragone plot. This device with a cell voltage of 1.7 V can reach a high energy density of 29.67 Wh kg<sup>-1</sup> at a low power density of 0.07 kW kg<sup>-1</sup> at 0.3 A g<sup>-1</sup>. Also it confirms that the CMK-3-150-15Co symmetric supercapacitor devices can maintain an energy density >10 Wh/kg even at a high power density.

#### 4. Conclusions

In summary, the post-synthetic approach was employed to fabricate CoO functionalized nanoporous carbon electrode materials by incipient wetness impregnation method for supercapacitor application. This approach proved to be an effective in controlling the amount of loading inside the mesochannels of the nanoporous carbon. The XRD results revealed that nanoporous architecture is maintained even after the incorporation of the huge amount of CoO inside the nanochannels of the nanoporous carbon support whereas the N<sub>2</sub> adsorption-desorption analysis confirmed a high surface area, huge pore volume and large pore diameter in the samples after the functionalization. Based on the HRSEM, HRTEM and STEM-HAADF study, it has been concluded that the CoO nanoparticles were finely distributed along the mesochannels of the nanoporous carbon with a well-ordered porous structure and the crystallinity and the size of the nanoparticles could be controlled by the simple adjustment of the concentration of the initial precursor solution. Through the electrochemical analysis of the resultant electrodes, CMK-3-150 with 15 wt% loading of CoO demonstrated superior supercapacitive performance with a maximum specific capacitance of 331 F g<sup>-1</sup> with high capacity retention (91%) after 5000 consecutive cycles. This excellent performance is due to the nanometer-sized CoO formed inside the CMK-3-150 with excellent textural parameters. The enhanced electrochemical supercapacitive performance of the CoO functionalized nanoporous carbon is attributed to the combined effect of EDLCs and pseudocapacitor offered by the mesoporous carbon support and the CoO nanoparticles, respectively. A symmetric supercapacitor cell based on CMK-3-150-15Co electrode has also been developed and it can maintain an energy density >10 Wh/kg even at a high power density.

#### Notes and references

- <sup>a</sup>AIBN, The University of Queensland, Brisbane 4072, Queensland, Australia. Fax: +61-7-3346-3973; Email: a.vinu@uq.edu.au
- <sup>b</sup>International Center for Materials Nanoarchitectonics, National Institute for Materials Science-1 Namiki, Tsukuba 305-0044, Ibaraki, Japan.
- <sup>c</sup>Petrochemical Research Chair, Department of Chemistry, King Saud University, Riyadh, Saudi Arabia.
- 1 A. S. Arico, P. Bruce, B. Scrosati, J. M. Tarascon and W. V. Schalkwijk, *Nat. Mater.*, 2005, **4**, 366.
  - 2 P. Simon and Y. Gogotsi, *Nat. Mater.*, 2008, **7**, 845.
  - 3 M. Winter and R. J. Brodd, *Chem. Rev.*, 2004, **104**, 4245.
  - 4 L. H. Bao, J. F. Zang and X. D. Li, *ACS Nano*, 2011, **11**, 1215.
  - 5 R. Kotz and M. Carlen, *Electrochim. Acta*, 2000, **45**, 2483.
  - 6 B. E. Conway, V. Birss and J. Wojtowicz, *J. Power Sources*, 1997, **66**, 1.
  - 7 R. Kötz and M. Carlen, *Electrochim. Acta*, 2000, **45**, 2483.
  - 8 J. S. Huang, B. G. Sumpter and V. Meunier, *Angew. Chem. Int. Ed.*, 2008, **47**, 520.
  - 9 D. S. Dhawale, A. Vinu and C. D. Lokhande, *Electrochim. Acta*, 2011, **56**, 9482.
  - 10 V. D. Patake, S. M. Pawar, V. R. Shinde, T. P. Gujar and C. D. Lokhande, *Curr. Appl. Phys.*, 2010, **10**, 99.
  - 11 K. Liang, X. Tang and W. Hu, *J. Mater. Chem.*, 2012, **22**, 11062.
  - 12 S. G. Kandalkar, D. S. Dhawale, C. K. Kim and C. D. Lokhande, *Synth. Met.*, 2010, **160**, 1299.
  - 13 D. P. Dubal, D. S. Dhawale, T. P. Gujar and C. D. Lokhande, *Appl. Surf. Sci.*, 2011, **257**, 3378.
  - 14 L. L. Zhang and X. S. Zhao, *Chem. Soc. Rev.*, 2009, **38**, 2520.
  - 15 J. R. Miller and P. Simon, *Science*, 2008, **321**, 651.
  - 16 V. Subramanian, H. Zhu and B. Wei, *J. Power Sources*, 2006, **159**, 361.
  - 17 M.-S. Balogun, W. Qiu, W. Wang, P. Fang and X. Lu and Yexiang Tong, *J. Mater. Chem. A*, 2014, DOI: 10.1039/c4ta05565a.
  - 18 M. Zhi, C. Xiang, J. Li, M. Li and N. Wu, *Nanoscale*, 2013, **5**, 72.
  - 19 M.E. Plonska-Brzezinska, D.M. Brus, A. Molina-Ontoria and L. Echegoyen, *RSC Adv.*, 2013, **3**, 25891.
  - 20 Y. Hou, J. C. Ndamanisha, L. Guo, X. Peng and J. Bai, *Electrochim. Acta*, 2009, **54**, 6166.
  - 21 H. Liu, S. Bo, W. Cui, F. Li, C. Wang and Y. Xia, *Electrochim. Acta*, 2008, **53**, 6497.
  - 22 J. Xu, P. Liu, Y. Lu, J. Zhao, J. Feng, Y. Song and B. Tang, *Adv. Mater. Resea.*, 2011, **239-242**, 1026.
  - 23 A. Vinu, V. Murugesan, W. Bohlmann and M. Hartmann, *J. Phys. Chem. B*, 2004, **108**, 11496.
  - 24 K.P.S. Prasad, D. S. Dhawale, T. Sivakumar, S. S. Aldeyab, J. SM. Zaidi, K. Ariga and A. Vinu, *Sci. Technol. Adv. Mater.*, 2011, **12**, 044602.
  - 25 S. Jun, S. H. Joo, R. Ryoo, M. Kruk, M. Jaroniec, Z. Liu, T. Ohsuna, O. Terasaki, *J. Am. Chem. Soc.*, 2000, **122**, 10712.
  - 26 R. Ryoo, S. H. Joo, M. Kruk, M. Jaroniec, *Adv. Mater.*, 2001, **13**, 677.
  - 27 R. Kotz and M. Carlen, *Electrochim. Acta*, 1999, **45**, 2483.
  - 28 S. Yoon, J. Lee, T. Hyeon and M. Oh, *J. Electrochem. Soc.*, 2000, **147**, 2507.
  - 29 M. Dai, L. Song, J. T. LaBelle and B. D. Vogt, *Chem. Mater.*, 2011, **23**, 2869.
  - 30 D. S. Dhawale, M. R. Benzigar, M. A. Wahab, C. Anand, V. Shaji, V. V. Balasubramanian, S. S. Aldeyab, K. Ariga and A. Vinu, *Electrochim. Acta*, 2012, **77**, 256.
  - 31 D.S. Dhawale, G.P. Mane, S. Joseph, C. Anand, K. Ariga, A. Vinu, *ChemPhysChem* **2013**, **14**, 1563.
  - 32 C. Xiang, M. Li, M. Zhi, A. Manivannan and N. Wu, *J. Mater. Chem.*, 2012, **22**, 19161.
  - 33 M. Zhi, A. Manivannan, F. Meng and N. Q. Wu, *J. Power Sources*, 2012, **208**, 345.
  - 34 D. Hulicova, M. Kodama and H. Hatori, *Chem. Mater.*, 2006, **18**, 2318.
  - 35 C. M. A. Brett and A. M. O. Grett, *Electrochemistry: Principles, Methods, and Applications*, Oxford University Press, Oxford, 1993.

- 36 A. J. Bard and L. R. Faulkner, *Electrochemical Methods: Fundamentals and Applications*, 2<sup>nd</sup> ed., John Wiley & Sons, Inc., 2001.
- 37 B.C. Jones, A.F. Hollenkamp, and S.W. Donnea, *J. Electrochem. Soc.*, 2010, 157, p. A551.

## Cobalt oxide functionalized nanoporous carbon electrodes and their excellent supercapacitive performance

Dattatray S. Dhawale,<sup>a,b</sup> Gurudas P. Mane,<sup>b</sup> Stalin Joseph,<sup>a</sup> Siddulu N. Talapaneni,<sup>b</sup> Chokkalingam Anand,<sup>a,b</sup> Ajayan Mano,<sup>b</sup> Salem S. Aldeyab,<sup>c</sup> Kripal S. Lakhi,<sup>a</sup> and Ajayan Vinu\*<sup>a,b</sup>

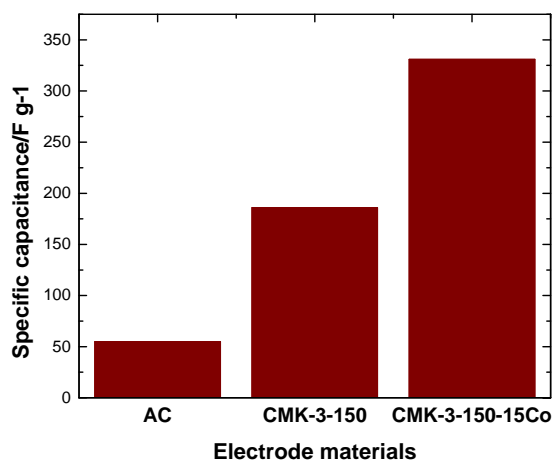


**Fig. S1.** Variation specific capacitance of AC, CMK-3-150 and CMK-3-15-15Co electrodes.